Simulation Studies of Combustion in a Constant-Mass Variable-Volume Combustion Chamber

Lucky Anetor
Professor
Nigerian Defence Academy
Department of Mechanical Engineering
Kaduna
Nigeria

Edward E. Osakue
Associate Professor
Texas Southern University
Department of Industrial Technologies
Houston, Texas
USA

A numerical simulation code was used to conduct a systematic study of the effects of fuel-air equivalence ratios in the range $0.7 \leq \phi \leq 1.4$ and compression ratio, $r_c = 8.0$ on key operating parameters, such as pressure, rate of change of pressure, '∕dt' flame extinction temperature, burn rate frequency, combustion efficiency, η_b, source term, mass burn fractions and heat loss in a simulated 5.734 liter, V8 spark-ignition engine. The data shows that the burn rate characteristics of the fuel and oxidizer are qualitatively perfectly correlated. The results also show that as flame extinction/flameout is approached, the fuel consumption rate, R_{fu} increases rapidly with temperature for fuel-air equivalence ratios, ϕ in the range $0.7 \leq \phi \leq 1.4$. The average burn rate frequency (per second), $f_{br}(1/s)$ varies from $11.2 \leq f_{br} \leq 137.0$ for fuel-air equivalence ratios, ϕ in the range $0.7 \leq \phi \leq 1.4$ The results further show that the fastest fuel consumption rate was for fuel-air equivalence ratio, $\phi = 1.4$ in the time interval, t such that $0.0 \leq t \leq 0.61$ ms while the slowest corresponds to $\phi = 0.7$ and the corresponding time interval was $0.0 \leq t \leq 3.98$ ms. Moreover, the data shows that for fuel-air equivalence ratios, ϕ in the range $0.7 \leq \phi \leq 1.4$ the fuel consumption rate increases monotonically after the initial ignition delay period. The combustion efficiency, η_b of the engine under investigation were found to be in the range of $94.1\% \leq \eta_b \leq 94.4\%$ for lean mixtures, that is, for $\phi < 1.0$;the corresponding values of combustion efficiency, η_b for fuel-rich mixtures were in the interval $93.8\% \leq \eta_b \leq 94.1\%$. The other results from this study are summarized in the conclusion.

Keywords: Fuel-air equivalence ratio, compression ratio, extinction flame temperature, burn rate frequency, combustion efficiency, engine knock, activation energy

1. INTRODUCTION

The main source of environmental pollution in urban centers of the world can be traced to emissions produced by vehicles which are powered by internal combustion engines (ICEs). These pollutants originate from non-ideal combustion processes which are common in internal combustion engines and their formation is influenced byboth the engine operating parameters (for example, engine temperature, speed, load, air-fuel ratio, ignition delay, spark timing, exhaust gas recirculation, etc.) as well as the fuel composition. Internal combustion engine emissions consist of volatile organic compounds (*VOCs*), carbon monoxide (*CO*), nitric oxide (*NO*) and nitrous oxide (NO_2) which are collectively referred toas oxides of nitrogen (NO_X), particulate matter (PM), carbon dioxide (CO_2) and water vapor (H_2O). Volatile organic compounds (*VOCs*) and (NO_X) form photochemical smog in the atmosphere, and (*CO*) and (*PM*) have been identified as having adverse health effect on human beings.

The impacts of fossil fuel combustion permeate many areas of our lives, in particular, it relatestothe economy, sustainability, variation of climatic conditions and energy utilization. In view of the foregoing issues, research efforts are now been concentrated on designing cost effective, safe, efficient and non-polluting combustion devices for a variety of fossil fuels with a view to keeping cost reasonable while protecting the environment and sustaining our standard of living.

A thorough understanding of combustion at a fundamental and engineering perspective is required so as to be able to improve the design of engine combustion systems. Detailed understanding of engine combustion is a difficult undertaking that entails a comprehensive knowledge of the chemical sciences, thermodynamics, heat transfer, fluid dynamics and advanced mathematics. For example, a complete comprehension of the most elementary turbulent flame requires detailed knowledge of turbulent reacting flow, a phenomenon which is highly intractable and is presently an active area of rigorous research efforts.Since it is impossible to wait until such a time that adequate knowledge of combustion dynamicsin ICE is attained, engineers who are tasked with designing combustion devices have turned to using a combination

Received: January 2018, Accepted: March 2018
Correspondence to: Dr Lucky Anetor,
Department of Mechanical Engineering,
Nigeria Defence Academy, Kaduna, Nigeria
E-mail: lanetor@uh.edu
doi:10.5937/fmet1804475A

of science, experimentation, numerical simulation and experience in order to look for practicable solutions.In choosing the thermodynamic models that are normally used for engine combustion simulations we rely on some implicit understanding of the physical and chemical mechanisms they contain. Since the description of the most relevant and important aspects of the engine processes are usually incorporated into these models, the models have been found to performed extremely well and they are ideally suited for initial parametric studies

Numerical modeling of internal combustion (reci–procating and rotary) engines involve thermodynamics, fluid mechanics, turbulence, heat transfer, combustion, chemical reactions and numerical analysis. In simulating the ICE, various levels of approximation have been used to predict the performance of internal combustion engines. Studies range from simple air standard cycles to complex three dimensional models which employ turbulence, chemical reactions, spray dynamics, heat transfer models, etc. In general, the numerical models of internal combustion engine can be classified into four categories, namely, zero-dimensional single zone, zero-Dimensional/one-Dimensional single zone models, quasi-dimensional multi-zone models and multidimensional models. In zero-one-Dimensional models, the ICE is represented as a network of pipes (intake and exhaust manifolds) with "devices" that simulate different parts of the machine (valves, cylinders, pipe junctions, etc.) interconnecting them. For zero-dimensional models, the vast majority of the properties are averaged over the total volume of the combustion chamber and there is no spatial information.

A zero-dimensional single-zone model is capable of predicting engine performance and fuel economy accurately with a high computational efficiency. The major weakness of single-zone models is their inability to accurately simulate wave propagation into pipes and manifolds which the volumetric efficiency strongly depend upon. Furthermore, these models cannot account for the temporal and spatial variation of temperature and fuel spray in the mixture. It is worth mentioning that both the temporal and spatial variation of temperature and fuel spray is crucial in predicting harmful species formed during the combustion process.

In view of the foregoing, multi-dimensional models, such as the KIVA family of Fortran-based Computational Fluid Dynamics code which was developed by Los Alamos National Laboratory [1] is being used to resolve the combustion chamber space into fine grids, thus providing a considerable amount of spatial information. However, multi-dimensional models still employ phenomenological sub-models to describe physical processes such as fuel spray, turbulence, combustion, etc. that are present during the combustion process.

There is presently an intermediary method between zero-dimensional and multi-dimensional models that is called quasi-dimensional. Multi-zone models [2]can be effectively used to simulate innovative engine combus–tion systems, by combining the advantages of zero-dimensional models and multi-dimensional models. These models are capable of providing the spatial information required to predict emission products with minimal requirement on computing resources.

2. LITERATURE REVIEW

The current pressure on automotive engine manu–facturers to improve on internal combustion engine's fuel efficiency while simultaneously achieving acceptable emission levels has encouraged a lot of research activities in this field. The reviewspresented in this section describe various strategies that are presently beingused to study ICE combustion processes.

It is a well-known fact that heat transfer affects the performance and phasing of internal combustion engines. Empirical relationships and equilibrium wall-function models are usually employed in engine simulations to predict wall heat transfer. However, numerous studies have shown that significant errors usually occur due to the failure of the underlying assumptions employed in deriving these equilibrium wall-function models. Non-equilibrium wall-function models have been found to provide a more accurate way of predicting the near-wall region heat transfer of in-cylinder flows.

In order to buttress this fact, [3]conducted a study in which simultaneous high-speed high-resolution particle image velocimetry and heat-flux measurements were employed in an optically accessible engine. The experiments were performed under both motored and fired conditions at two different engine speeds. The experimental data were utilized to assess the performance of different heat transfer models in predicting the thermo-viscous boundary layer. These models include commonly used heat transfer correlations, equilibrium and modified wall-function models and the non-equilibrium wall model which was recently developed. It was found that the equilibrium wall-function significantly under predicts the heat flux under both motored and fired conditions whereas, the non-equilibrium wall model was found to adequately capture the structure and dynamics of both momentum and thermal boundary layers in comparison with experimental measurements. It was concluded that the performance of the non-equilibrium wall model was superior to those of empirical correlation wall functions and the equilibrium model.

A quasi one-dimensional numerical code which was based on fuel–air cycle analysis was developed by[4]and used to predict the performance of two- and four-stroke fuel-inducted engines. The study was undertaken in order to provide boundary conditions for a finite element analysis which was used to predict thermal and mechanical loading of carbon–carbon pistons which was designed to be usedfor advanced internal combustion engine prototype. The simulation code was able to predict the required boundary conditions, namely, the gas pressure, temperature and heat transfer coefficients as a function of crank angle, as well as the indicated and brake power outputs, thermal efficiency and mean effective pressure. The code employs variable specific heat calculation throughout the operational cycle. The compression of an air–fuel–residual gas mixture was calculated followed by a finite

rate burn, where the burn duration was calculated on the basis of the turbulent flame speed and cylinder geometry. The authors also used the code to study the tendency for engine knock or auto-ignition. The authors concluded that the code produced results which were in good agreement with actual engine operational data.

Lucchini et al. [5] presented a comprehensive approach which was developed using an open-source computational fluid dynamics code. In order to minimize the pre-processing time and preserve the accuracy of the results, algorithms for automatic mesh generation of spray-oriented grids were developed and applied to different combustion chamber geometries. The Lagran–gian approach was used to describe the spray evolution while the combustion process was modeled by employing detailed chemistry and turbulence–chemistry interaction. The proposed numerical code was first tested by simulating cold flow thereafter; it was used to compute reacting flows in a constant-volume vessel, where the operating conditions mimicking those of heavy-duty diesel engines were simulated. Finally, the authors used their code to model two different load points and two piston bowl geometries. Experimental validations of these results were carried out by comparing the computed and experimental data with the cylinder pressure, heat release rate and pollutant emissions (NO_X, CO and UHC) of a real engine. The simulated results were found to reproduce the measured data reasonably well.

The other efforts that are actively being researched in order to provide better understanding of combustion efficiency and effective control of combustion emi–ssions can be found in references [6–14]and the refe–rences contained in them.

This paper is organized as follows; the introduction is presented in section 1, followed by the literature review in section 2. Section 3 presents the objectives of the present study, while section 4 details the engine simulation model while the modeling of the combustion process is described in section 5. The details concerning the setup and implementation of the numerical solution, initial and boundary conditions applied, internal consis–tency checksand convergence criteria are presented in section 6. The results of the parametric studies are pre–sented in section 7. Finally, the conclusions are presented in section 8.

3. OBJECTIVE OF THE PRESENT STUDY

The control and optimization of combustion are crucial to fulfilling various legislations concerning the environ–ment and the future enhanced performance required of internal combustion engines. Increasing break mean effective pressure at high loads and extending the operating range of advanced combustion engines appear to be the most promising way of reducing fuel consum–ption and pollutant emissions simultaneously. In view of this, comprehensive computational fluid dynamics tools are usually used to predict the complex interactions of the various phenomenological processes, such as fuel–air mixing, unsteady diffusion combustion and for–mation of noxious species prevailing within the combustion chamber of an ICE. Detailed kinetics, consistent spray models and high quality grids are usually necessary in order to perform high quality predictive and parametric simulation studies which can be used either for design or diagnostic purposes. In view of the foregoing, the objective of this study is to use chemical kinetics and various fuel-air equivalent ratios to investigate the variation of concentration of products of combustion and tempe–rature within the combustion chamber of an ICE. The ultimate goal of this work is to gainsome understanding of combustion characteristics in ICEs in order to be able to optimize the design of future engines.

4. THE ENGINE CYCLE SIMULATION MODEL

In an internal combustion engine a substantial portion of the combustion processes take place when the inlet and exhaust valves are closed simultaneously. Since there is no inflow or outflow, we can model this situation as a constant-mass combustion reactor/bomb with temporal variation of mixture properties. The equations descri–bing the combustion processes can therefore be reduced to their zero-dimensional, unsteady models. It is worth mentioning that the volume of a constant-mass combus–tion reactor/bomb may or may not have temporal variation.

As stated above, the objective of the present study is to model constant-mass combustion reactor, as for example, in ICE by simplifying the unsteady, three-dimensional equations which are given below.

This will facilitate the computation of the time history of the reacting mixture from its initial reactant state to its final product state. In general, the product state may or may not be in equilibrium. The main utility of these simplified models are to provide a means of studying the fundamental physics behind the combus–tion processes in these devices. The results obtained from these models cannot be depended upon solely for practical designs; however, they do provide guidance on the main dynamics inherent in the constant-mass combustion reactor/bomb.

4.1 Conservation of mass equation

The law of conservation of mass for bulk fluid mixtures is given by:

$$\frac{\partial(\rho_m)}{\partial t}+\frac{\partial(\rho_m u_j)}{\partial x_j}=0 \tag{1}$$

where ρ_m is the mixture density, u_j is the fluid velocity with j = 1,2,3, x_j is the coordinate in three mutually perpendicular directions and t is the time.

4.2 Conservation of species

The equation of mass transfer of the species can be written as:

$$\frac{\partial(\rho_m\omega_k)}{\partial t}+\frac{\partial(\rho_m u_j\omega_k)}{\partial x_j}=\frac{\partial}{\partial x_j}\left(\rho_m D\frac{\partial\omega_k}{\partial x_j}\right)+R_k \tag{2}$$

where k is the number of species, ω is the mass fraction, D is the mass diffusivity and R_k is the volumetric gene–ration rate from chemical reaction.

When Equation (2) is summed over all species k of the mixture; Equation (1) is obtained. This can be explained as follows: from Dalton's law, $\rho_m = \sum_k \rho_k$, since $\rho_k = \rho_m \omega_k$ and $\sum_k \omega_k = 1$ Moreover, $\sum_k N_{i,k} = \rho_m u_i$. Therefore, on summing over all species k, Equation (2) reduces to:

$$\frac{\partial \rho_m}{\partial t} + \frac{\partial \left(\rho_m u_j\right)}{\partial x_j} = \sum_k R_k \tag{3}$$

On comparing Equation (3) with Equation (1), Equation (3) becomes exactly equal to Equation (1) when $\sum_k R_k = 0$. The physical interpretation of this is that when some species are generated by for example a chemical reaction, some others are consumed. This implies that there is no net mass generation in the bulk fluid.

4.3 Conservation of chemical elements

It can be shown that the mass fraction η_α of chemical element α in the mixture of a chemical reaction mechanism containing k species, is given by [13]:

$$\eta_\alpha = \sum_k \eta_{\alpha,k} \omega_k \tag{4}$$

where $\eta_{\alpha,k}$ is the mass fraction of element α in species k. In a manner analogous to species convection, diffusion, generation and consumption/destruction so also are the elements in a chemical reaction. However, the chemical elements can neither be destroyed nor created/generated in view of the principle of conservation of element (law of definite proportions). Therefore, the transport equation for any chemical element α will have no source term. Hence, the conservation of element equation is given by:

$$\frac{\partial \left(\rho_m \eta_\alpha\right)}{\partial t} + \frac{\partial \left(\rho_m u_j \eta_\alpha\right)}{\partial x_j} = \frac{\partial}{\partial x_j}\left(\rho_m D \frac{\partial \eta_\alpha}{\partial x_j}\right) \tag{5}$$

Notice that the diffusion coefficient D for the elements is assumed to be equal to those of the species [14].

4.4 Energy equation

In combustion calculations, it is more convenient to use the enthalpy or the temperature forms of the energy equation. It can be shown that the energy equations in enthalpy and temperature forms are given by [15]:

$$\rho_m \frac{Dh_m}{Dt} = \frac{\partial}{\partial x_j}\left(k_{eff} \frac{\partial T}{\partial x_j}\right) - \frac{\partial \left(\sum m'_{j,k}{}' h_k\right)}{\partial x_j} + \\ + \ldots + \mu \Phi_v + \frac{Dp}{Dt} + \dot{Q}_{rad} + \dot{Q}_{others} \tag{6}$$

and the energy equation in terms of temperature is:

$$\rho_m c_{p_m} \frac{DT}{Dt} = \frac{\partial}{\partial x_j}\left(k_{eff} \frac{\partial T}{\partial x_j}\right) + \mu \Phi_v + \frac{Dp}{Dt} + \\ + \dot{Q}_{rad} + \dot{Q}_{others} - \sum_k h^0_{f,k} + \Delta h_{s,k} - \rho_m \sum_k D \frac{\partial \omega_k}{\partial x_j} \frac{\partial h_k}{\partial x_j} \tag{7}$$

where T is the temperature, c_{p_m} is the specifi heat at constant pressure of the mixture, h_m is the enthalpy of the mixture, h_k is the enthalpy of species k, $k_{eff} = k_m + k_t$ is the effective conductivity, k_m is the conductivity of the mixture and k_t is the turbulent conductivity, $\dot{Q}_{rad}$ and $\dot{Q}_{other}$ are the volumetric generation/dissipation from radiation and other sources respectively. The viscous dissipation function is Φ_v and μ is the molecular viscosity.

The following important remarks concerning the energy equation in temperature form are worth menti–oning:

1. $-\sum_k h^0_{fk} R_k = \dot{Q}_{chem}$ is the net volumetric rate of heat generation as a result of chemical reaction. For a simple chemical reaction (*SCR*), $\dot{Q}_{chem} = R_{fu} \Delta H_c$ where H_c is the enthalpy of formation.

2. If we assume that the specific heats of all species are equal, that is, $c_{p_j} = c_{p_m} = c_p$, then $\sum_k \Delta h_{s,k} \; R_k = 0$ The last term in Equation (7) is also zero because $\sum_k \mathbf{D} \, \partial \omega_k \big/ \partial x_j = 0$.

3. The viscous dissipation terms $\mu \Phi_v$ are significant only in high Mach number flows. Similarly, the Dp/Dt term is important in compressible flows particularly when shock waves are present.

5. MODELING COMBUSTION IN ICE

In internal combustion engines, the combustion taking place at the top dead center position can be modeled as a constant mass constant volume process whereas when the engine is in the normal operational mode, the combustion dynamics can be treated as a constant mass variable volume process.

In a spark ignition engine, the combustion of fuel-air mixture is initiated at the top dead center (TDC) position or at a few crank angle degrees before top dead center. The combustion process usually continues over quite a few crank angle degrees into the power stroke, however, the mass of the combustion products remain essentially constant while the combustion chamber volume changes. Furthermore, heat from the combusting gases is transferred to the coolant through the cylinder walls.

During normal operation of a spark ignition engine, the equation of bulk mass becomes:

$$\frac{d\left(\rho_m V\right)}{dt} = V \frac{d\rho_m}{dt} + \rho_m \frac{dV}{dt} = 0 \tag{8}$$

From [15], it can be shown that:

$$\frac{dV}{dt} = A_c \frac{dx_p}{dt} = A_c u_p \tag{9}$$

where:

$$V = A_c\left(x_0 + x_p\right), x_p = c\left(1-\cos\theta\right) + l - \sqrt{l^2 - c^2\sin^2\theta}$$

and $u_p = \frac{dx_p}{dt} = \left[1 + \frac{c\cos\theta}{l^2 - c^2\sin^2\theta}\right] c\Omega\sin^2\theta$.

$\Omega = 2\pi N/60$ is the angular velocity of the crank in *rad/s*, and N is in revolutions per minute and l and c are the lengths of the connecting rod and crank respectively, x_0 is the clearance height at TDC, x_p is the instantaneous position of the piston, A_c is the cross-sectional area of the combustion cylinder and u_p is the speed of the piston at any instant of time/crank angle.The crank angle, θ is measured clockwise and θ = 0 is the top dead center position while θ = 180° corresponds to the bottom dead center (BDC) position.

From the foregoing, Equation (8) can be expressed as:

$$\frac{d\rho_m}{dt} = -\rho_m \frac{A_c}{V} u_p = -\frac{\rho_m u_p}{x_0 + x_p} \tag{10}$$

Furthermore, by using Equation (8), Equations (9) and (10) simplify to:

$$\rho_m \frac{d\omega_j}{dt} = R_j, \quad j = F, OX, P \tag{11}$$

andthe energy equation becomes:

$$\frac{d\left(\rho_m V e\right)}{dt} = q_w A_w - \dot{W}_{\exp} = q_w A_w - p\frac{dV}{dt} \tag{12}$$

where $p\frac{dV}{dt}$ represents the work transfer by the pressure the combusting gases exert on the piston head, *F, OX* and *P* represent the fuel, oxidizer and combustion products respectively. Equation (12) can be further simplified to Equations (13) and (14):

$$\frac{d}{dt}\left[\rho_m V\left(h_m - \frac{p}{\rho_m}\right)\right] = q_w A_w - p\frac{dV}{dt} \tag{13}$$

$$\begin{aligned} &\frac{d}{dt}\left[\rho_m V h_m\right] = q_w A_w - p\frac{dV}{dt} + \frac{d}{dt}\left(pV\right) \Rightarrow \\ &\Rightarrow \rho_m V\frac{dh_m}{dt} = q_w A_w + V\frac{dp}{dt} \end{aligned} \tag{14}$$

where $e = h_m - p/\rho_m$ and $h_m = c_{p_m} T + \Delta H_c \omega_F$ Equation (14) can be transformed to:

$$\rho_m \frac{d}{dt}\left|c_{v_m} T\right| = q_w \frac{A_w}{V} + \Delta H_c \left|R_F\right| - p\frac{dV}{dt} \tag{15}$$

Therefore, the processes taking place in a spark ignitionengine can be modeled with Equations (10), (11), (14) and or (15).

In order to put a closure to this model it is necessary to stipulate physical models for wall heat transfer q_w and combustion product pressure p. In an internal combustion engine, the pressure-crank angle history is normally determined from in-cylinder measurements or the pressure could be obtained from:

$$p = \rho_m R_m T \tag{16}$$

where R_m is the gas constant for the mixture.

The wall heat transfer can be modeled as[16]:

$$\alpha = 0.035\frac{k_g}{d}\left(\frac{U_g d}{v_g}\right)^{0.8} \tag{17}$$

where the heat transfer coefficient α is usually obtained from measurements. It varies with time and locations along the surfaces of the engine combustion chamber. Because of this, spatially averaged coefficients are normally used for preliminary studies. The other variables appearing in Equation (17) are defined below:

$$U_g = 2.28\overline{u}_p + 0.00324V\left(p - p_{ad}\right)\frac{T_0}{p_0 V_0}$$

$$\overline{u}_p = 2b\frac{N}{60}$$

$$p_{ad} = p_0\left(\frac{V_0}{V}\right)^{\gamma}, \quad \gamma \cong 1.4$$

and the subscript g and 0 refer to gas and conditions at the BDC when intake valve closes, $\overline{u}_p$ is the mean piston speed, d is the diameter of the combustion chamber and p_{ad} is the isentropic compression or expansion pressure which obeys the relation $pV^{\gamma} = constant$.

For internal combustion engine studies, [17] recommend that the correlation given below should be used for α:

$$\alpha = 0.82 d^{-0.2} U_g^{0.8} p^{0.8} T^{-0.53} \tag{18}$$

The derivation of the models presented so far assume that temperature and mass fractions are uniform all over the combustion chamber volume at all times. That is, the state of the products of combustion is assumed to be isotropic; this type of representation is referred to as thermodynamic model. However, in practical combustion devices, the ignition process creates substantial spatial and temporal variations of temperature and mass fractions as the flame front propagates through the unburned mixture. Sometimes, the air-fuel mixture resulting from pressure and temperature rise during the compression stroke, may auto-ignite, thereby leading to engine knock, which most often causes substantial damage to the piston-crank assembly. It is for this reason that an accurate model of the rate of pressure rise is highly important.

5.1 Modeling ICE combustion dynamics as a constant mass variable volumeprocess

As stated above, in an internal combustion engine, ignition is initiated a few crank angle degrees BTC and

a greater portion of the fuel-air mixture is burnt at constant volume while the combustion of the remaining unburnt charge propagates further into parts of the expansion stroke. Therefore, strictly speaking, in a constant mass reactor, combustion can either be appro–ximated as a constant-volume or a variable-volume process. In the constant mass variable volume scenario, the combustion chamber volume, V will vary with time and it can be determined from the speed, N of the engine and the dimensions of the connecting rod and crank which are connected to the piston. In the present paper parametric studies of the effects of fuel-air equivalent ratio on pressure and temperature history as well as on the products of combustion was undertaken for the combustion processes in an internal combustion engine. Variable volume combustion chambermodels as well as appropriately transformed versions of Equations (1) to (18) were employed in the present work.

5.2 Simulation combustion in an ICE chamber as a constant-mass variable-volume reactor

The scenario used to illustrate the constant mass variable volume combustion process is as described and implemented below.

A mixture of *n*-octane, (C_8H_{18}) and moist air (ϕ = 1.0, x_{H2O} = 0.03) is drawn into an engine at $T = 300K$ and p = 1.01325 bar. The engine speed in revolutions per minute is 1400 *rpm.* The engine cylinder bore, d = 101.6 mm and stroke length, L = 88.4 mm. The crank radius, c = 44.2 mm, and connecting rod length, l = 144.92 mm. Assume that at TDC (or $\theta = 0$), the mass fractions and pressure correspond to T = 1000 K as calculated below. Assume a single step reaction model and T_w = 650 K. Investigate the time/crank angle histories of T,p and mass-fractions ω_f, ω_{O2}, ω_{CO2}, and ω_{H2O}, α, and q_w until the end of power stroke for equivalence ratios, $0.7 \leq \phi \leq 1.4$which is equivalent to air-fuel ratio, AFR, in the range; ($10.76 \leq AFR \leq 21.53$) and compression ratio, r_c = 8.0.The objective is to simulate the combustion of fuel-air mixture in a constant-mass variable volume combustion chamber until flame extinction (that is, fuel is totally consumed). Furthermore, the examination of heat loss, combustion efficiency, η_b and the corresponding crank angle at which the fuel or oxygen is totally consumed (that is, end of combustion) were also investigated.

In order to simulate the conditions described above and to keep computational effortssimple, the following assum–ptions regarding the thermodynamics and the chemical kinetics in the combustion chamber of an ICE were made:

1. One-step global kinetics and the following engineering approximation for global reaction was made [18]:

$$C_xH_y + \left(x + {y}/{4}\right)O_2 \xrightarrow{K_c} xCO_2 + \left({y}/{2}\right)H_2O \qquad (19)$$

$$\frac{d\left[C_xH_y\right]}{dt} = -A_F \exp\left(-\frac{E_a}{R_uT}\right)\left[C_xH_y\right]^m\left[O_2\right]^n \qquad (20)$$

where $[*][*] \triangleq {kmol}/{m^3}\cdot s$.

For normal octane: AF = 4.049 × 10^{10}, ${E_a}/{R_u} = 20131$, m = 0.25, n = 1.5, k_G is the global rate coefficient, E_a is the activation energy, R_u is the universal gas constant, T is temperature in Kelvin, m and n are exponential parameters, x and y are the number of carbon and hydrogen atoms respectively in the fuel.

2. The specific heats at constant pressure of the fuel, air and products are constant and equal, that is, $c_{pF} = c_{pOX} = c_{pP} = 1200\frac{J}{kg}\cdot K$ and the mole–cular weight of the mixture, M_m = 29.
3. Isentropic compression, that is, γ = 1.4 is assumed. Furthermore, it was assumed that $c_{pj} = c_{pm} = 1200\frac{J}{kg}\cdot K$ and mixture molecular mass, M_m = 29.
4. In the present study stoichiometric air-fuel ratio is 15.05 and combustion is constrained to stichio–metric or lean burn conditions.

The value of the parameters, A, ${E_a}/{R_u}$, m and n were chosen in such a manner that they give the best agre–ement when experimental and predicted flame speeds and flammability limits are compared [19].

Comments

a. The use of global kinetics is hard to justify for modeling combustion in spark ignition engines. However, the only justification for using this model was to illustrate principles while acknowledging that our results may not be very precise. In order to achieve more compre–hensive results, computational fluid dynamics codes such as [20] are normally used.
b. Assumptions 2 and 3 provide values that give reasonable estimates.

6. NUMERICAL SOLUTION

In order to simulate the situation described in section 5.2, we proceed as follows:

For the case under consideration, Equation (11) transforms to:

$$\frac{d\left(\omega_{C_8H_{18}}\right)}{dt} = -\frac{\left|R_{C_8H_{18}}\right|}{\rho_m} \qquad (21)$$

$$\frac{d\left(\omega_{O_2}\right)}{dt} = -\frac{\left|R_{O_2}\right|}{\rho_m} \qquad (22)$$

$$\frac{d\left(\omega_{CO_2}\right)}{dt} = -\frac{\left|R_{CO_2}\right|}{\rho_m} \qquad (23)$$

$$\frac{d\left(\omega_{H_2O}\right)}{dt} = -\frac{\left|R_{H_2O}\right|}{\rho_m} \qquad (24)$$

$$\frac{d\left(\omega_{N_2}\right)}{dt}=0 \tag{25}$$

From Equation (12), we get:

$$\rho_m\frac{de}{dt}=q_wA_w-p\frac{dV}{dt}\Rightarrow\frac{d}{dt}\left(h_m-\frac{p}{\rho_m}\right)= \\ =\rho_m\frac{d}{dt}\left(c_{p_m}T+\Delta H_c\omega_{C_8H_{18}}-R_{mix}T\right)=q_wA_w-p\frac{dV}{dt}, \tag{26}$$

or

$$\Rightarrow\rho_m\frac{d}{dt}\left(c_{v_m}T\right)+\left[\rho_m\frac{d\left(\omega_{C_8H_{18}}\right)}{dt}\right]\Delta H_c=q_wA_w-p\frac{dV}{dt}$$

where $c_{v_m}=c_{p_m}-R_{mix}$

Therefore:

$$\frac{d}{dt}\left(c_{v_m}T\right)=\frac{q_wA_w}{\rho_m}-\frac{p}{\rho_m}\frac{dV}{dt}+\frac{\Delta H_c}{\rho_m}\left|R_{C_8H_{18}}\right| \tag{27}$$

From the foregoing, the net consumption rate of C_8H_{18} is given by:

$$\left|R_{C_8H_{18}}\right|=MW_{C_8H_{18}}\times\left|-A_F\exp\left(-\frac{E_a}{R_uT}\right)\left[C_8H_{18}\right]^{0.25}\left[O_2\right]^{1.5}\right| \\ \Rightarrow\left|R_{C_8H_{18}}\right|=\left|-A_F\exp\left(-\frac{E_a}{R_uT}\right)\rho_m^{1.75}\cdot\frac{MW_{C_8H_{18}}^{0.75}}{MW_{O_2}^{1.5}}\cdot\omega_{C_8H_{18}}^{0.25}\cdot\omega_{O_2}^{1.5}\right| \tag{28}$$

Since a single-step global mechanism which also referred to as simple chemical reaction is assumed in the present study, then:

1 *kg* of fuel + r_{st} *kg* of oxygen → (1 + r_{st}) *kg* of products (29)

Where r_{st} is the stoichiometric ratio and is defined as:

$$r_{st}=\frac{MW_{O_2}}{MW_F},\quad a_{stoic}=\frac{MW_{O_2}}{MW_F}\left(m+\frac{n}{4}\right)$$

Therefore:

$$R_{O_2}=r_{st}R_F\ \text{ and }\ R_p=-\left(1+r_{st}\right)R_F \tag{30}$$

From the stoichiometric combustion of *n*-octane, (C_8H_{18})

$$R_{O_2}=r_{st}R_{C_8H_{18}}\text{ and }R_{CO_2}=R_{H_2O}=-\left(1+r_{st}\right)R_{C_8H_{18}}$$

On combining Equations (21) to (27), we get:

$$\frac{\dot{Q}_{rad}}{\dot{Q}_{others}} \tag{31}$$

$$\left[\omega_{C_8H_{18}}-\frac{\omega_{CO_2}}{\left(1+r_{st}\right)}\right]_t=\left[\omega_{C_8H_{18}}+\frac{\omega_{CO_2}}{\left(1+r_{st}\right)}\right]_i \tag{32}$$

$$\left[\omega_{C_8H_{18}}+\frac{\omega_{H_2O}}{\left(1+r_{st}\right)}\right]_t=\left[\omega_{C_8H_{18}}+\frac{\omega_{H_2O}}{\left(1+r_{st}\right)}\right]_i \tag{33}$$

$$\left[\omega_{C_8H_{18}}+\frac{c_{v_m}}{\Delta H_c}T\right]_t=\left[\omega_{C_8H_{18}}+\frac{c_{v_m}}{\Delta H_c}T\right]_i \tag{34}$$

From Equations (31) to (34), $\omega_{C_8H_{18}},\omega_{O_2},\omega_{CO_2}$ and ω_{H_2O} can be expressed as functions of temperature *T*, when their initial reactant values are known. The initial values are solved for as follows:

The initial reactants, R_{react} are:

$$R_{react}=C_8H_{18}+\frac{12.5}{\phi}\left(O_2+3.76N_2\right)+n_{H_2O}H_2O$$

where n_{H2O} is the initial number of moles of water vapor, H_2O. The mole fraction, x_{H2O} of water vapor is given by:

$$\frac{n_{H_2O}}{1+12.5\times4.76/\phi+\eta_{H_2O}}=x_{H_2O}=0.03 \\ \Rightarrow n_{H_2O}=1.87113 \tag{35}$$

Therefore, the initial reactant mass, MRi = 114 + 12.5(32 + 3.76 × 28) + 1.8711 × 18 = 1863.68.

Hence, $\omega_{C_8H_{18}}=114/1863.68=0.06117$ similarly, $\omega_{O_{2_i}}=0.21463$, $\omega_{N_{2_i}}=0.70613$ and $\omega_{H_2O_i}=0.01807$ and $\omega_{CO_{2_i}}=0$.

With the initial values/conditions known, Equation (27) becomes:

$$\frac{d}{dt}\left(c_{v_m}T\right)=\left[\left|R_{C_8H_{18}}\right|\frac{\Delta H_c}{\rho_m}+\frac{q_wA_w}{\rho_m}-\frac{p}{\rho_m}\frac{dV}{dt}\right] \tag{36}$$

where:

$$\omega_{C_8H_{18}}=\omega_{C_8H_{18_i}}-\frac{c_{v_m}}{\Delta H_c}\left(T-T_i\right)$$

$$\omega_{O_2}=\omega_{O_{2_i}}+r_{st}\left(\omega_{C_8H_{18}}-\omega_{C_8H_{18_i}}\right)$$

$$\Rightarrow\omega_{O_2}=\omega_{O_{2_i}}-r_{st}\frac{c_{v_m}}{\Delta H_c}\left(T-T_i\right)$$

$$\omega_{CO_2}=\omega_{CO_{2_i}}-\left(1+r_{st}\right)\left(\omega_{C_8H_{18}}-\omega_{C_8H_{18_i}}\right)$$

$$\Rightarrow\omega_{CO_2}=\left(1+r_{st}\right)\frac{c_{v_m}}{\Delta H_c}\left(T-T_i\right)$$

$$\omega_{H_2O}=\omega_{H_2O_i}-\left(1+r_{st}\right)\left(\omega_{C_8H_{18}}-\omega_{C_8H_{18_i}}\right)$$

$$\Rightarrow\omega_{H_2O}=\omega_{H_2O_i}+\left(1+r_{st}\right)\frac{c_{v_m}}{\Delta H_c}\left(T-T_i\right)$$

In order to complete the modeling of the right hand side (RHS) of Equation (36), we have to model the values of ρ_m, c_{v_m} and ΔH_c as well. These quantities are modeled as:

$\Delta H_c=(H_{reaction}-H_{product})_T$, similarly, the adiabatic flame temperature, T_{ad} is computed for the combustion temperature T and equivalent ratio, ϕ. While the extinction temperature, T_{ext} corresponds to the value of $\omega_{C_8H_{18}}$ such that $\omega_{C_8H_{18}}=0$.

$c_{v_m}=\sum_j\omega_jc_{v_j}=\sum_j\left(c_{p_j}-R_u/M_j\right)$, where c_{p_j} is ev–aluated as a function of temperature, *T* at each instant of

time during the computation of Equation (36). Finally, $\rho_m = {pM_m}/{(R_u T)}$, where $M_m = \left(\sum_j {\omega_j}/{M_j} \right)^{-1}$. The volume is computed as shown in Equation (37),

$$\left(\frac{pV}{R_m T} \right)_{t+\Delta t} = \left(\frac{pV}{R_m T} \right)_t \tag{37}$$

From Equation (37), the instantaneous values of can be computed. Furthermore, Equation (36) can now be expressed as:

$$\left(c_{v_m} T \right)_{t+\Delta t} = \left(c_{v_m} T \right)_c + RHS\left(T_c \right) \cdot \Delta t \tag{38}$$

In the present study the Euler's integration computational method was used to solve the resulting model, that is, Equation(38), at every instant of time. The time-step, Δt which was used in this study was 10^{-5} s. However, Δt was gradually reduced as $T^* = (T\text{-}T_i)/(T_{ad} - T_i) \rightarrow 1.0$, in order to preserve accuracy. Simulations were terminated when $\omega_{C_8H_{18}} \leq 0$ and the flame is extinguished, that is fuel is totally consumed.

6.1 Initial conditions

In order to complete the necessary input information, the relevant initial conditions for the first order differential equation which describes the interactions between temperature, pressure and mass fractions are specified thus:

- Initial conditions - temperature: $T = T_i = T_{amb} \cdot (rc)^{0.4}$ at $t = 0$
- Initial conditions - pressure: $p = p_i = p_{amb} \cdot (rc)^{1.4}$ at $t = 0$
- Initial conditions - mass fraction of species: at $t = \left\{ \omega_{C_8H_{18}}, \omega_{O_2}, \omega_{CO_2} \textbf{ and } \omega_{H_2O} \right\}_{i'}$ refer to Equation (35).

6.2 Convergence criteria

For the zero dimensional model used in the present study, convergence was obtained after 21 iterations at each time step. The local truncation, discretization and global errors are on the order of $O(\Delta t^2)$, $O(\Delta t)$ and $O(\Delta t)$ respectively for the Euler integration scheme. In view of these, convergence criterion was set to a tolerance value of 10^{-6}. Therefore, complete calculations are repeated until the final values converge to within the specified tolerance with the initial values.

7. RESULTS

The results presented in this study were obtained from a simulated 5.734 liter, V8 engine. Table 1 below lists the engine specifications, operating conditions and fuel input parameters.

The data presented shows the temporal variation of several important parameters which are useful for characterizing the performance of internal combustion engines at various fuel-air equivalence ratios, ϕ. The quantities are combustion chamber pressure, rate of change of combustion chamber pressure with time, combustion chamber temperature, combustion efficiency, η_b, flame extinction temperature, heat lossand variation of mass fractions of fuel, water vapor, carbon dioxide and oxidizer. The operating conditions investigated are clearly annotated in Figures 1 - 12.

Comprehensive discussions of how well the model reproduces the effects of fuel-air equivalence ratio on the combustion characteristics mentioned aboveare presented in the paragraphs that follow.

Table 1. Engine specifications

Parameter	Value
Number of cylinders, n_c	8
Bore (mm)	101.6
Stroke (mm)	88.4
Crank radius (mm)	44.2
Crank radius/connecting rod ratio, ε	0.305
Connecting rod length mm	144.92
Compression ratio, r_c	8.0
Engine speed (rpm)	1400
Inlet valves diameter (mm)	50.8
Inlet valves maximum lift (mm)	10.0
Inlet valves opens (°*CA AT DC*)	357
Inlet valves closes (°*CA AT DC*)	-136
Exhaust valves diameter (mm)	39.6
Exhaust valves maximum lift (mm)	10.0
Exhaust valves opens (°*CA AT DC*)	116
Exhaust valves closes (°*CA AT DC*)	371
Valve overlap (degrees)	14°
Cylinder wall temperature, $T_w(K)$	650
Initial temperature, $T(K)$	848.16
Fuel, *n*-octane	C_8H_{18}
Fuel-air equivalence ratios, ϕ	$0.7 \leq \phi \leq 1.4$

Figures 1 and 2 show the variation of mass burn fraction of fuel and oxygen with time for fuel-air equivalence ratios, ϕ in the range $0.7 \leq \phi \leq 1.4$. The data shows that the burn rate characteristics of the fuel and oxidizer are qualitatively perfectly correlated. The characteristics in Figures 1 and 2 show that as flame extinction/flameout is approached, the fuel consumption rate, R_{fu} increases rapidly with temperature (see Figures 3 and 4) for fuel-air equivalence ratios, ϕ in the range $0.7 \leq \phi \leq 1.4$. Figure 1shows that the average burn rate frequency (per second), f_{br}(1/s) varies from $11.2 \leq f_{br} \leq 137.0$ for fuel-air equivalence ratios, ϕ in the range $0.7 \leq \phi \leq 1.4$. This is due to the fact that, in a fuel-lean mixture, the flame extinction/flameout limit is governed by the fuel mass fraction.Whereas, in a fuel-rich mixture the flame extinction/flameout limit is controlled by the oxygen mass fraction. It is worth mentioning that in a fuel-rich mixture, the assumption of a single-step reaction is not strictly valid due to dissociation. Therefore, in order to have a closure (that is, the equality of number of equations and the number of species) the water–gas reaction must be included in the reaction mechanism. The visual evidence of the foregoing is clearly captured in Figures 1 and 2.

The variation of fuel consumption rate and flame temperature with time for fuel-air equivalence ratios, ϕ in the range $0.7 \leq \phi \leq 1.4$ are shown in Figures 3 and 4.

Figure 3 shows that the fastest fuel consumption rate is for fuel-air equivalence ratio, ϕ = 1.4in the time interval, t such that $0.0 \leq t \leq 0.61$ ms while the slowest corresponds to ϕ = 0.7 and the corresponding time interval is $0.0 \leq t \leq 0.61$ ms. Moreover, Figure 3 shows that for fuel-air equivalence ratios, ϕ in the range $0.7 \leq \phi \leq 1.4$, the fuel consumption rate increases monoto–nically after the initial ignition delay period.

Furthermore, Figure 3 shows that the fuel consum–ption rate is highly dependent on the fuel-air equivalent ratio.The computer model used for this study accurately replicate these trends which have been observed in actual internal combustion engine experimental measu–rements[19]. Figures 3 and 4 showthat after the initial flame development time intervals, which correspond to $0.0 \leq t \leq 0.61$ ms, $0.0 \leq t \leq 0.79$ ms, $0.0 \leq t \leq 1.11$ ms and $0.0 \leq t \leq 3.98$ ms for fuel-air equivalence ratios 1.4, 1.2, 1.0, 0.8 and 0.7 respectively, the remaining charge in the combustion is then consumed almost instan–taneously as evidenced in the rapid rise in flame temperature shown in Figure 4. As can be seen from Figure 4 the time rate of change of temperature is stee–pest for fuel-air equivalence ratio, ϕ = 1.4 and least for ϕ = 0.7.

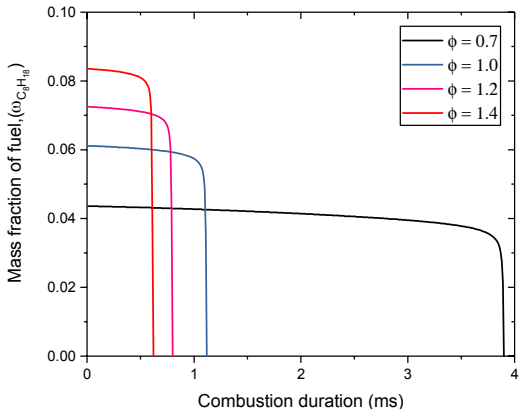

Fig. 1: Variation of mass burn fraction of fuel with time for fuel-air equivalence ratios, $0.7 \leq \phi \leq 1.4$.

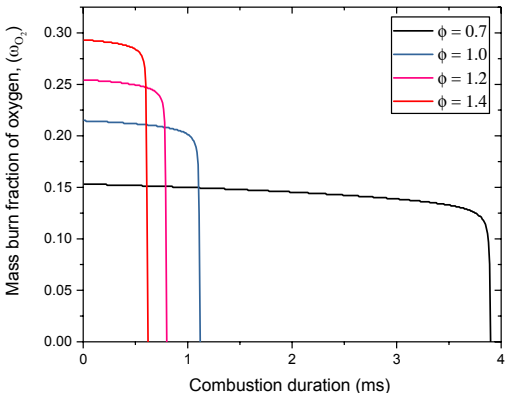

Fig. 2: Graph of mass burn fraction of oxygen with time for fuel-air equivalence ratios, $0.7 \leq \phi \leq 1.4$.

The temporal variation of the characteristics of combustion chamber pressure and rate of change of pressure for fuel-air equivalence ratios, ϕ in the range $0.7 \leq \phi \leq 1.4$ are shown in Figures 5 and 6 respec–tively.The figures show that as fuel-air equivalence ratio increases the pressures and the rate of change of pressure increases proportionately as well. However, it can be seen from Figure 5 that at fuel-air equivalence ratios in the range $0.8 \leq \phi \leq 1.4$, the rise in both pressure and rate of change of pressure are quite smooth and somewhat gradual for most portions of the combustion processes, thereafter, a rapid consumption of the remaining charge ensues. However, for fuel-air equivalence ratio ϕ = 0.7 the pressure characteristics decrease over the flame development time interval and then recover somewhat during the final period of spontaneous charge consumption. This could be attributed to the fact that substantial amount of heat was transferred to the combustion wall due to very slow charge consumption rate.

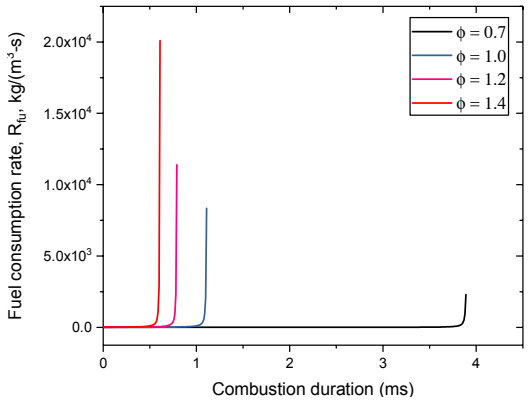

Fig. 3: Graph of fuel consumption rate with time for fuel-air equivalence ratios, $0.7 \leq \phi \leq 1.4$.

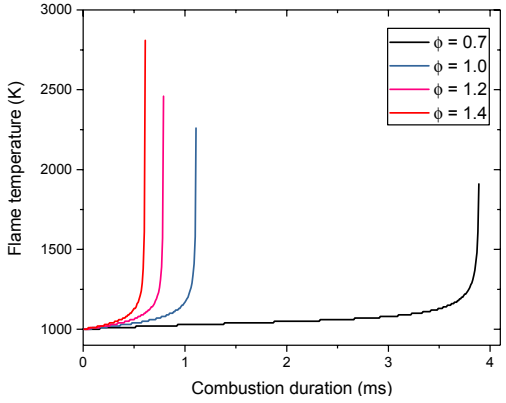

Fig. 4: Graph of flame temperature versus time for fuel-air equivalence ratios, $0.7 \leq \phi \leq 1.4$.

The shapes of the pressure and rate of change of pressure as combustion progresses (Figures 5 and 6) are positively correlated with the temperature characteristics (Figure 4) for fuel-air equivalence ratios, $0.8 \leq \phi \leq 1.4$, except for the case where ϕ = 0.7. The possible reason for this deviation was stated above.

The results show that it took about 0.61, 0.79, 1.11, 1.89 and 3.98 ms for fuel-air equivalence ratios 1.4, 1.2, 1.0, 0.8 and 0.7 respectively, for the in-cylinder combustion dynamics to reach T* = 1.0. In the last 0.01 ms, for all the fuel-air equivalence ratios investigated the rate of change of pressure, $\frac{dp}{dt}$ lies in the range

$3.23 \times 10^{10} \leq dp/dt \leq 2.19 \times 10^{11}$ Pa/s, while the corres–ponding flame temperatures vary within the limit $1910 \leq T \leq 2810$ K. The rapid change in temperature and pressure with corresponding high rate of consum–ption of fuel-oxidizer (C_8H_{18} - O_2) mixture characterizes thermochemical explosion, that is, engine knock. This phenomenon is due to the extremely fast interaction between the energy released and the corresponding temperature rise from the combustion reaction which in turn feeds back to produce constantly increasing reaction rates because of the dependence of temperature on the reaction rate, that is, ($-E_a/RT$), where E_a is the activation energy.

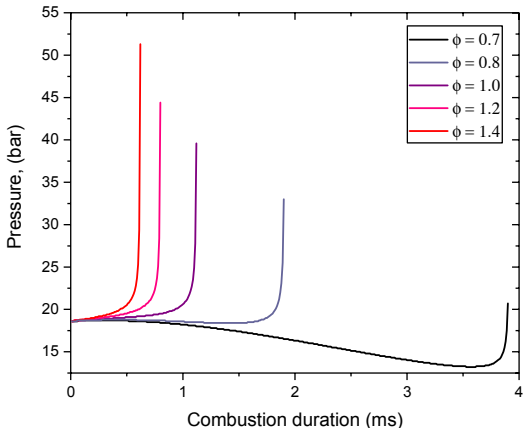

Fig. 5: Graph of pressure versus time for fuel-air equivalence ratios, $0.7 \leq \phi \leq 1.4$.

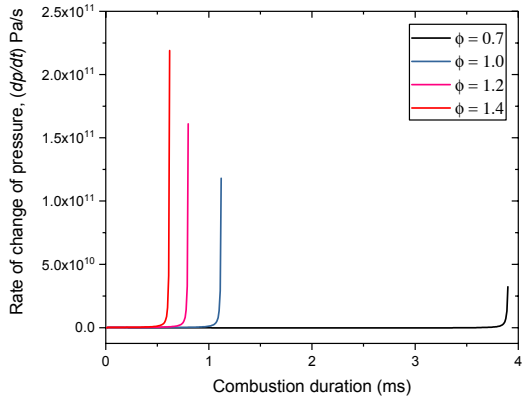

Fig. 6: Graph of rate of change of pressure versus time for fuel-air equivalence ratios, $0.7 \leq \phi \leq 1.4$.

The results of flame extinction temperatures versus fuel-air equivalence ratios, ϕ in the range $0.7 \leq \phi \leq 1.4$ are shown in Figure 7. Figure 7 shows that flame extinction temperatures are positively correlated with fuel-air equivalence ratios. Furthermore, the data show that the simulated temperatures are fairly higher than those typically observed in real internal combustion engines for fuel-air equivalence ratios, ϕ in the range $1.2 \leq \phi \leq 1.4$. This discrepancy could be attributed to the fact that the effects of wall quenching and radiation were not taken into consideration in the present model since the model was largely designed for initial preliminary/exploratory studies.

The characteristics presented in Figures 4, 7 and 8 can be summarized as follows; increasing fuel concen–tration and temperature results in an increase in flame temperature with concomitant increase in the rate of energy generation. Conversely, when the concentration of oxidizer is reduced, flames with high values of fuel concentration and temperature will require high convective energy losses to induce flame extinction. Equally true; flames with low fuel concentration and temperature are more predisposed to kinetic extinction. Flame extinction is a factor limiting combustion perfor–mance in internal combustion engines. Some of the techniques such as advanced fuel-air mixing strategies exhaust gas recirculation (EGR) and staged injections which are used for achieving low emissions in ICEs can be adversely affected by flame extinction. Flame ex–tinction is highly influenced by the operating conditions, for example, local fuel-air equivalence ratio and the reaction kinetics of the fuel. The studies of flame extinction are central to flame characterization and response analysis. Furthermore, such studies do provide data for validation of kinetic reaction mechanisms.

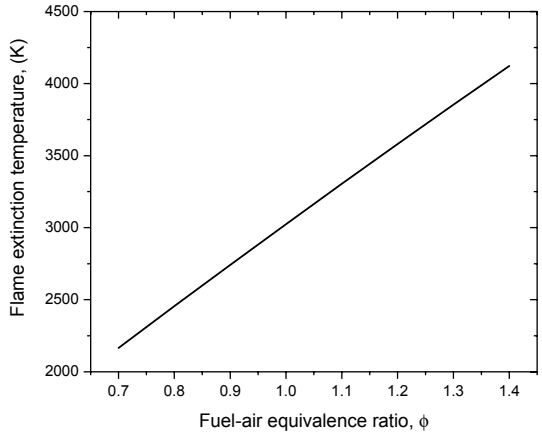

Fig. 7: Graph of flame extinction temperature versus fuel-air equivalence ratios, $0.7 \leq \phi \leq 1.4$.

High performance engines and propulsion systems frequentlyoperate at extreme conditions near or below the flammability boundary in order to improve energy efficiency and reduce emission. The flammability limit is governed by fuel kinetics and flame radiation. Due to the preferential diffusion effect, fuels with smaller Lewis numbers can burn beneath the flammability limit if strained. That is, a strained/stretched flame can burn leaner than un-strained flames. In summary, flame ex–tinction temperature can serve as a guide to the impact of fuel composition on the extinction strain rate.

Figure 8 shows the graph of the variation of the source term (heat release rate) with combustion duration for fuel-air equivalence ratios, $0.7 \leq \phi \leq 1.4$. From Figure 8 it can be seen that the source term is highest for fuel-air equivalence ratio of $\phi = 1.4$ and least for $\phi = 0.7$ with the magnitudes of other source terms in between, that is, source terms for fuel-air equivalence ratios, $1.0 \leq \phi \leq 1.4$.Furthermore, Figure 8 shows that the leaner a fuel-air mixture is, the longer it takes to burn. It can also be seen from Figure 8 that little changesin fuel-air equivalence ratio, ($\phi \sim 0.1$) lead to significant changes in the heat release rate. This observation is due to the fact that the relationship

between chemical reaction rate and the equivalence ratio is highly non-linear, especially at lean conditions, that is, at $\phi < 1.0$. One of the most important properties of a combustion process is the heat release rate since it characterizes the amount of thermal energy that can be obtained from the oxidation of a fuel/hydrocarbon. The spatial distribution of the source term (heat release rate) is able to provide information concerning localized hot spots which can be used to identify areas of the combustion chamber which might be susceptible to uncontrolled ignition. Moreover, the source term (heat release rate) is very important for understanding and predicting combustion instability.

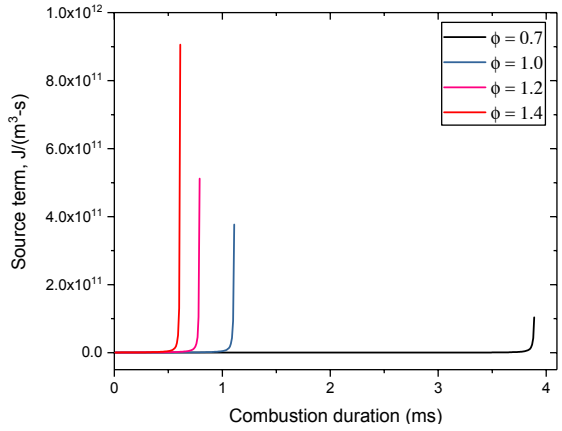

Fig. 8: Graph of source term with time for fuel-air equivalence ratios, $0.7 \leq \phi \leq 1.4$.

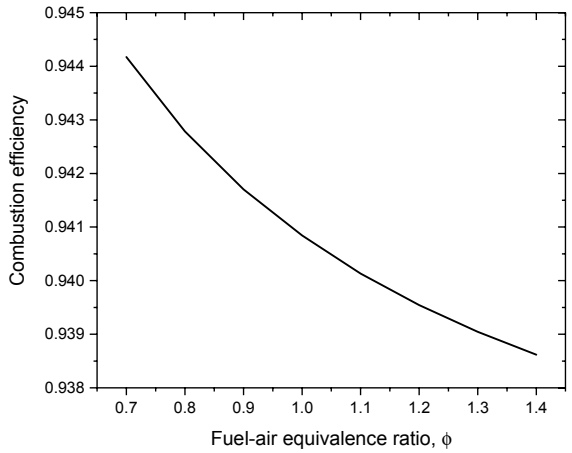

Fig. 9: Graph of combustion efficiency versus fuel-air equivalence ratios, $0.7 \leq \phi \leq 1.4$.

Figure 9 shows the result of combustion efficiency versus fuel-air equivalence ratios, ϕ in the range $0.7 \leq \phi \leq 1.4$. From Figure 9 we can see that combustion efficiency, η_b of the engine under investigation are in the range of $94.1\% \leq \eta_b \leq 94.4\%$ for lean mixtures, that is, for $\phi < 1.0$. Furthermore, since there is insufficient air for complete oxidation of all the fuel in fuel-rich mixtures, that is, for $\phi > 1.0$, the combustion efficiency steadily decreases as the mixture strength becomes richer. As shown in Figure 9, the values of combustion efficiency, η_b for fuel-rich mixtures are in the interval $93.8\% \leq \eta_b \leq 94.1\%$. In internal combustion engines combustion efficiency is to a very large extent inde–pendent of other engine operating and design variables, as long as the engine combustion process remains stable. It is worth mentioning that, in general, comp–ression ignition engines often operate lean and typically have combustion efficiencies of approximately 98%.

It is the combustion dynamics elucidated in Figure 9 that provided the impetus for employing lean combus–tion in most combustion technology applications, such as boilers, burners, furnaces, gas turbines and com–bustion chambers of internal combustion engines. The various areas of applications mentioned above most often strive to take advantage of the fact that combus–tion processes operating under lean fuel conditions, that is, $\phi < 1.0$ do have very high combustion efficiency and impressively low emission levels. Since the flame temperatures are generally very low, pollutant formation and emissions such as, NO_X are usually very low.

Furthermore, when lean-burn is carried out with excess air for hydrocarbon oxidation, complete combu–stion of the fuel normally follows, with a concomitant reduction in unburned hydrocarbon and carbon monoxide emissions. However, because of slow reac–tion dynamics, instabilities, extinction, low heat release rate and sensitivity to mixing that usually characterize lean-burn conditions, the realization of these impro–vements and achieving the requirements of real com–bustion systems is usually a formidable undertaking.

In general, the characteristics shown in Figure 9 and similar ones can be used to explore the performance of state-of-the-art combustion technologies utilizing fuel-air equivalence ratios, $\phi < 1.0$ and their advantages in achieving present and future requirements of com–bustion systems.

The characteristics shown in Figure 10 is the relationship between heat loss and combustion duration for fuel-air equivalence ratios, $0.7 \leq \phi \leq 1.4$. in the internal combustion engine been studied. Figure 10 shows that for fuel-air equivalence ratios, ϕ in the range $0.7 \leq \phi \leq 1.4$, the rate of heat loss during the combustion period increases monotonically with fuel-air equiva–lence ratio. This could be due to the fact that as the fuel-air equivalence ratio increases the combustion chamber wall and residual gas temperatures increase as well. Furthermore, higher temperatures during the engine cycle results in copious production of radicals during the early stages of combustion; this can sometimes lead to auto-ignition. It is worth stating that maximum temperature and rate of heat loss for the engine under consideration appear to occur at an equivalence ratio of $\phi = 1.4$. From various measurements that have been carried out on real engines and other practical combustion devices, maximum temperature and hence rate of heat loss has often occurred on the rich side of stoichiometric. A plausible explanation for this is as follows: for equivalence ratios, $\phi \leq 0.7$, the combustion process is limited by the amount of fuel available whereas at equivalence ratios, $\phi > 1.0$, the oxidation process is governed by the quantity of oxygen available.

At intermediate equivalence ratios, that is, $0.7 \leq \phi \leq 1.4$ the combustion process is constrained somewhat by the ease of forming free radicals. It can then be

surmised that operating an internal combustion engine slightly rich implies that there is sufficient fuel available to realize this. The interactions of these factors combine to cause the observed characteristics of the rate of heat loss for equivalence ratios in the interval $0.7 \leq \phi \leq 1.4$.

As stated above the maximum rate of heat loss occurs at an equivalence ratio, $\phi = 1.4$ which is higher than for most spark ignited engines which have equivalence ratio, $\phi = 1.1$. This may have to do with the fact that turbulence, mixing characteristics of the combustion chamber and radiative heat loss were not included in our model.

The graphs of mass fractions of carbon dioxide (CO_2) and water vapor (H_2O) produced versus combus–tion durationfor fuel-air equivalence ratios, $0.7 \leq \phi \leq 1.4$. are shown in Figures 11 and 12 respectively. The graphs show that the trends are positively correlated to a very high degree with fuel consumption rate, see Figure 3. It can be seen from Figures 11 and 12 that the least amount of carbon dioxide (CO_2) and water vapor (H_2O) were produced at fuel-air equivalence ratios in the range, $0.7 \leq \phi \leq 1.0$. This could be due to that fact that the combustion duration was somewhat slow with the concomitant low rate of the carbon dioxide (CO_2) and water vapor (H_2O) production.

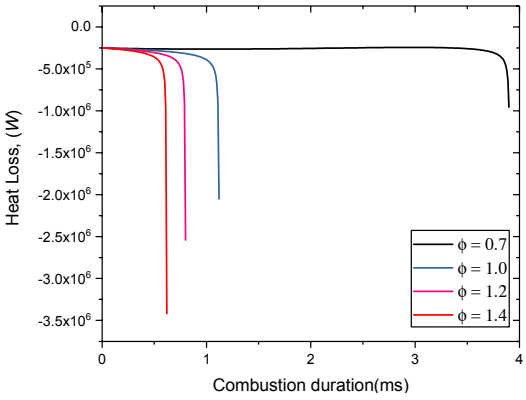

Fig. 10: Graph of heat loss versus time for fuel-air equivalence ratios $0.7 \leq \phi \leq 1.4$.

8. CONCLUSION

A numerical simulation code was used to investigate the effects of fuel-air equivalence ratio on some of the important performance characteristics of a 5.734 liter, V8 spark-ignition engine. The combustion process is based on a constant mass variable volume thermo–dynamic model. The simulation results are valuable in the initial conceptual design phase, during experimental /testing analysis and in diagnosing field problems.

The trends of ICE performance characteristics captured by this code were quite similar both qualitatively and quantitatively to their experimentally observed counterparts. The findings from this study gave a comprehensive insight into the relationship between equivalence ratio and the engine performance characteristics investigated in this study. The results are shown in Figures 1 to 12.

In specifics, the conclusions from this study can be summarized as follows:

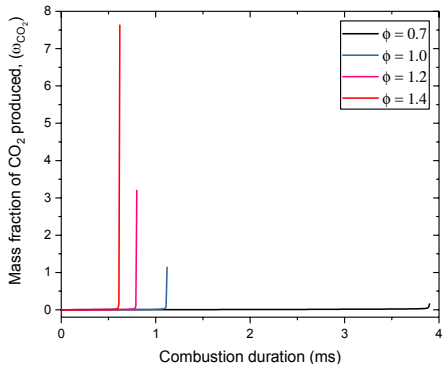

Fig. 11: Graph of mass fraction of carbon dioxide produced versus time for fuel-air equivalence ratios, $0.7 \leq \phi \leq 1.4$.

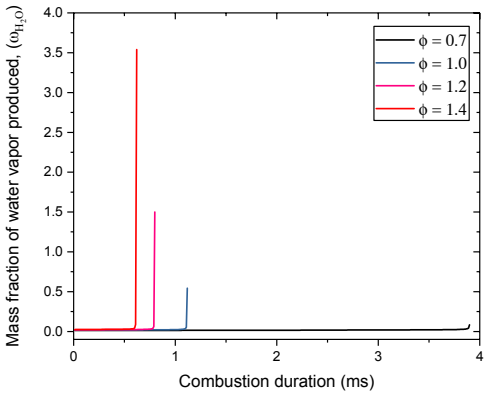

Fig. 12: Graph of mass fraction of water vapor produced versus time for fuel-air equivalence ratios, $0.7 \leq \phi \leq 1.4$.

1. The model used in this study can be used to investigate the variation of key operating parameters, such as pressure, rate of change of pressure, dp/dt flame extinction temperature, combustion efficiency, η_b, source term, mass burn fractions and heat loss with fuel-air equivalence ratio, ϕ.
2. The data shows that the burn rate characteristics of the fuel and oxidizer are qualitatively perfectly correlated. The results also show that as flame extinction/flameout is approached, the fuel consumption rate, R_{fu} increases rapidly with tempe–rature for fuel-air equivalence ratios, ϕ in the range $0.7 \leq \phi \leq 1.4$.
3. The present work shows that the ignition delay periods for the various fuel-air equivalence ratios ($0.7 \leq \phi \leq 1.4$) range from about $6° \leq CAD \leq 33°$
4. The average burn rate frequency (per second), f_{br}(1/s) varies from $11.2 \leq f_{br} \leq 137.0$ for fuel-air equivalence ratios, ϕ in the range $0.7 \leq \phi \leq 1.4$.
5. The results show that the fastest fuel consumption rate was for fuel-air equivalence ratio, $\phi = 1.4$ in the time interval $0.0 \leq t \leq 0.61$ ms while the slowest corresponds to $\phi = 0.7$ and the corresponding time interval was $0.0 \leq t \leq 3.98$ ms Moreover, the data shows that for fuel-air equivalence ratios, ϕ in the range $0.7 \leq \phi \leq 1.4$ the fuel consumption rate increases monotonically after the initial ignition delay period.
6. The computed characteristics show that after the initial flame development time intervals, which correspond to $0.0 \leq t \leq 0.61$ ms, $0.0 \leq t \leq 0.79$ ms,

$0.0 \leq t \leq 1.11$ ms and $0.0 \leq t \leq 3.98$ ms for fuel-air equivalence ratios 1.4, 1.2, 1.0, 0.8 and 0.7 respec–tively, the remaining charge in the combustion chamber was then consumed almost instanta–neously as evidenced in the rapid rise in flame temperature shown in Figure 4. As can be seen from Figure 4 the time rate of change of tempe–rature is steepest for fuel-air equivalence ratio, $\phi = 1.4$ and least for $\phi = 0.7$.

7. The results show that as fuel-air equivalence ratio increases the pressures and the rate of change of pressure increases proportionately as well. However, it can be seen from Figure 5 that at fuel-air equivalence ratios in the range $0.8 \leq \phi \leq 1.4$, the rise in both pressure and rate of change of pressure are quite smooth and somewhat gradual for most portions of the combustion processes, thereafter, a rapid consumption of the remaining charge ensues. Conversely, for fuel-air equivalence ratio $\phi = 0.7$ the pressure characteristics decrease over the flame development time interval and then recover some–what during the final period of spontaneous charge consumption.
8. The results show that it took about 0.61, 0.79, 1.11, 1.89 and 3.98 ms for fuel-air equivalence ratios 1.4, 1.2, 1.0, 0.8 and 0.7 respectively, for the in-cylinder combustion dynamics to reach $T^* = 1.0$. In the last 0.01 ms, for the all fuel-air equivalence ratios investigated the rate of change of pressure, dp/dt lies in the range $3.23 \times 10^{10} \leq \mathrm{dp/dt} \leq 2.19 \times 10^{11}$ Pa/s, while the corresponding flame temperatures vary within the limit $1910 \leq T \leq 2810$ *K*.
9. The data shows that the simulated temperatures were fairly higher than those typical observed in real internal combustion engines for fuel-air equivalence ratios, ϕ in the range $0.7 \leq \phi \leq 1.4$.
10. The simulated results show that the source term is highest for fuel-air equivalence ratio of $\phi = 1.4$ and least for $\phi = 0.7$. Furthermore, Figure 8 shows that the leaner a fuel-air mixture is, the longer it takes to burn.
11. The data shows that combustion efficiency, η_b of the engine under investigation are in the range of $94.1\% \leq \eta_b \leq 94.4\%$ for lean mixtures, that is, for $\phi < 1.0$; the corresponding values of combustion effi–ciency, η_b for fuel-rich mixtures were in the interval $93.8\% \leq \eta_b \leq 94.1\%$
12. Figure 10 shows that for fuel-air equivalence ratios, ϕ in the range $0.7 \leq \phi \leq 1.4$., the rate of heat loss during the combustion period increases monoto–nically.
13. Figures 11 and 12 show that the least amount of carbon dioxide (CO_2) and water vapor (H_2O) were produced at fuel-air equivalence ratios in the range, $0.7 \leq \phi \leq 1.0$.

ACKNOWLEDGEMENTS

The work reported herein was graciously supported by the Nigerian Defence Academy, Kaduna, Nigeria and Texas Southern University, Houston, Texas, USA. The authors wish to express their sincere thanks to their colleagues and reviewers for their insightful and const–ructive remarks, which led to improving the clarity and quality of this paper.

NOMENCLATURE

c_{p_m}	Specific heat at constant volume of the mixture
c_{v_m}	Specific heat at constant volume of the mixture
D	Mass diffusivity
E_a	Activation energy
h_k	Enthalpy of species k
h_m	Enthalpy of the mixture
k	Number of species
$k_{eff} = k_m + k_t$	Effective conductivity
k_m	Conductivity of the mixture
k_t	Turbulent conductivity
k_G	Global rate coefficient
M_m	Mixture molecular mass
N	Engine speed in revolutions per minute (rpm)
P	Engine combustion chamber pressure in bar
$\dot{Q}_{rad}$ and $\dot{Q}_{others}$	Volumetric generation/dissipation from radiation and other sources
r_c	Compression ratio
R_k	Volumetric generation rate from chemical reaction
R_u	Universal gas constant
T	Temperature in K
u_j	Fluid velocity
x_j	Coordinate in the three mutually perpendicular directions, j = 1,2,3
t	Time variable

GREEK SYMBOL

ΔH_c	Heat of combustion
ϕ	Fuel-air equivalence ratio
$\mathbf{\Phi}_v$	Viscous dissipation function
μ	Molecular viscosity
ω	Mass fraction

REFERENCES

[1] Torres, D.J., and M.F. Trujillo,KIVA-4: An unstructured ALE code for compressible gas flow with sprays, Journal of Computational Physics (219): 943-975, 2006.

[2] Kodavasal, J., Keum, S., Assanis, D. N., and A. Babajimopoulos, An Extended Multi-Zone Combu–stion Model for PCI Simulation, 21st International Multidimensional Engine Modeling User's Group Meeting, Detroit, MI, 2011.

[3] Ma P., Greene M., Sick V., Ihme M.: Non-equilibrium wall-modeling for internal combustion engine simulations with wall heat transfer, Inter–national J of Engine Research, Vol. 18(1-2) 15–25, 2017.DOI: 10.1177/1468087416686699.

[4] Micklow, G. J., Owens, B., and M. Russell, Cycle analysis for fuel-inducted internal combustion

engine configurations,Proceeding of the Institution of Mechanical Engineers, (215): Part D, 2000.

[5] Lucchini, T. L., Augusto, D., Torre, G. D., Angelo, O., Noud, M., Lambertus, M. T. S., and A. Gilles, Comprehensive methodology for computational fluid dynamics combustion modeling of industrial diesel engines, International J of Engine Research: 1–13, 2017. DOI: 10.1177/1468087416679570.

[6] Pickett, V., Caton, J. A., Musculus, M. P. B., and A. E. Lutz.Evaluation of the equivalence ratio–temperature region of diesel soot precursor formation using a two-stage Lagrangian model, Int. J. Engine Res. (7): 349-368, 2006.

[7] Syed, Y., Venkateswarlu, K., and G. R. K. Sastry, Effect of Compression Ratio and Equivalence Ratio on the Emission Characteristics of a Hydrogen-Ethanol Fuelled Spark Ignition Engine, International Journal of Advanced Science and Technology (40), 2012.

[8] Kim, J., Bae, C., and G. Kim,The Effects of Spark Timing and Equivalence Ratio on Spark-Ignition Linear Engine Operation with Liquefied Petroleum Gas, SAE Technical Paper 2012-01-0424.

[9] Michele, B., Muhammad, A. C., Evatt, R. H., and K. Sanghoon, Modeling combustion under engine combustion network Spray A conditions with multiple injections using the transported probability density function method, International Journal of Engine Research: 1-9, 2017.

[10]Alireza, M., Timothy, J., Mark, P., and E. John, Prediction of air–fuel ratio control of a large-bore natural gas engine using computational fluid dynamic modeling of reed valve dynamics, International Journal of Engine Research: 1–9, 2017. DOI: 10.1177/1468087416686224.

[11] Manente, V., Johansson, B., and W. Cannella, Gasoline partially premixed combustion, the future of internal combustion engines?, International Journal of Engine Research, (12): 194-208, 2011. DOI: 10.1177/1468087411402441.

[12]Prasad, S. S., Robert, J. M., Dennis, N. A., Claus, B., and B. M. Jason,A thermodynamic model for homogeneous charge compression ignition combustion with recompression valve events and direct injection: Part I – Adiabatic core ignition model, International Journal of Engine Research: 1–20, 2016. DOI: 10.1177/1468087416664635.

[13]Hamann, H. et al, Efficiency scaling method of gasoline engines for different geometries and the application in hybrid vehicle simulation, International J of Engine Research: 1-20, 2016. DOI: 10.1177/1468087416667130.

[14]Raghuram, P., Ramkumar, P., and S. Suhan, Estimation of Air-Fuel ratio (AFR) in a Spark-Ignition (SI) Engine From Cylinder Pressure Measurements. IJRRAS 13 (3): 707-715, 2012.

[15]Anil, W. Date,*Analytic Combustion - With Thermo–dynamics, Chemical Kinetics, and Mass Transfer*. 32 Avenue of the Americas, New York, NY 10013-2473, USA, 2011. ISBN 978-1-107-00286-9, 2.

[16]Kays, W. M., M. E. Crawford, *Convective Heat and Mass Transfer. 3rd ed*., McGraw-Hill, New York, 1993.

[17]Borman, G. L., and K. W. Ragland,*Combustion Engineering*. McGraw-Hill, New York, 1998.

[18]Westbrook, C. K., and F. L. Dryer, Simplified Reaction Mechanisms for the Oxidation of Hydrocarbon Fuels in Flames, Combustion Science and Technology (25): 219-235, 1981.

[19]Heywood, B. John,*Internal Combustion Engine Fundamentals*. New York, McGraw-Hill, ISBN 0-07-100499-8, 1998.

[20]Torres DJ and Trujillo MF. KIVA-4: An unstructured ALE code for compressible gas flow with sprays. Journal of Computational Physics, vol. 219, pp. 943-975, 2006.

ПРОУЧАВАЊЕ СИМУЛАЦИЈЕ САГОРЕВАЊА У КОМОРИ ЗА САГОРЕВАЊЕ ПРИ КОНСТАНТНОЈ МАСИ И ПРОМЕНЉИВОЈ ЗАПРЕМИНИ СМЕШЕ ГОРИВА И ВАЗДУХА

Л. Анетор, Е. Е. Осакуе

Код за нумеричку симулацију користили смо за систематско проучавање ефеката једнаких вредности односа у смеши гориво-ваздух у опсегу $0,7 \leq \phi \leq 1,4$ и степена компресије r_c на кључне радне параметре: притисак, брзину промене притиска, *'/dt'* температуру гашења пламена, брзину тока сагоревања, ефикасност сагоревања$\eta_б$, продукте сагоревања, масене фракције горива и губитак топлоте, код симулације рада бензинског мотора V8 (5734 л). Подаци показују да постоји врло добра квалитативна корелација између карактеристика брзине сагоревања смеше и средства за оксидисање. Резултати такође показују да се са приближавањем гашења пламена брзина потрошње горива $P_{фу}$ убрзано повећава са температуром смеше, при чему јеφ у распону од $0,7 \leq \phi \leq 1,4$. Просечна брзина сагоревања (по секунди) f_{br} (1/s) варира у опсегу $11,2 \leq f_{br} \leq 137,0$ код смеше, ϕ је у опсегу$0,7 \leq \phi \leq 1,4$. Даље, резултати показују да је најбржа потрошња горива $\phi = 1,4$ у временском интервалу t тако да је $0,0 \leq m \leq 0,61$ *ms*, док је најспорија потрошња φ – 0,7 а одговарајући временски интервал је $0,0 \leq t \leq 3,98$ *ms*. Осим тога, према подацима за све односе гориво-ваздух у једнаким количинама, заφ у опсегу $0,7 \leq \phi \leq 1,4$, брзина потрошње горива монотоно расте после почетног периода одлагања паљења. Утврђено је да се ефикасност сагоревања η_bкод мотора који смо проучавали кретала у опсегу $94,1\% \leq \eta_b \leq 94,4\%$ за све смеше са релативно малим процентом горива, тј. за $\phi < 1,0$; одговарајуће вредности за ефикасност сагоревања η_b за све смеше са већим процентом горива кретале су се у интервалу $93,8\% \leq \eta_b \leq 94,1\%$. Остали резулати су приказани у закључцима овога рада.